Oct 23rd, 12:00 AM

A Numerical Model for Fire-exposed Composite Steel/concrete Slabs

Ralph Hamerlinck

Leen Twilt

Jan W. B. Stark

Tenth International Specialty Conference on Cold-formed Steel Structures
St. Louis, Missouri, U.S.A., October 23-24, 1990

A NUMERICAL MODEL FOR FIRE–EXPOSED COMPOSITE STEEL/CONCRETE SLABS

Ralph Hamerlinck[1], Leen Twilt[2] and Jan Stark[3]

SUMMARY

This paper deals with the influence of fire exposure on the behaviour of composite steel/concrete slabs. A model for numerical simulation of such behaviour has been developed. The model comprises a thermal model, a mechanical model for cross–sectional analysis and a mechanical model for structural analysis. The models have been experimentally verified.

INTRODUCTION

Structures that are applied in buildings have to meet fire–safety requirements. Normally these structures are judged on the basis of standard fire tests [1]. However, such tests are very expensive and time–consuming, for which reason tools have been designed to determine the fire resistance of steel and concrete structures by calculation [2], [3]. In Europe, recommendations for composite steel/concrete slabs, cf. Fig.1, were introduced by the European Convention for Constructional Steelwork (ECCS) in 1983 [4]. With these recommendations the fire resistance of composite slabs can be quickly and simply calculated. No additional measures have to be taken and no calculation is required to achieve a fire resistance of 30 minutes. For fire resistances of 60 minutes and more, additional measures, such as additional reinforcement, insulating coatings or suspended ceilings, normally have to be taken, cf Fig. 2. The calculation method provides a satisfactory prediction of the fire resistance for a specific field of application, considering the great number of assumptions and simplifications. Nevertheless, a mathematical model is needed, by means of which the behaviour of fire–exposed composite slabs can be predicted on a more fundamental basis. Such a model has been developed at Eindhoven University of Technology.
The model comprises a thermal model, by which means temperature profiles are calculated as a function of fire–exposure time ([5], [6]), and a mechanical model by which means the mechanical response of the slab structure is calculated [7].
The mechanical model is divided into two submodels:

1. a submodel for analysing the cross–sectional behaviour, providing moment–curvature diagrams as a function of time, and
2. a submodel for analysing the structural behaviour, providing moment distributions and deflections as a function of time.

---

[1]Research Engineer, Structural Engineering Section, Eindhoven University of Technology, the Netherlands.

[2]Head Technical Centre for Fire Prevention, TNO Institute for Building Materials and Structures, Rijswijk, the Netherlands.

[3]Professor Steel Structures, Structural Engineering Section, Eindhoven University of Technology, the Netherlands and
Deputy Director, TNO Institute for Building Materials and Structures, Rijswijk, the Netherlands.

In the scope of an international research program, which is currently being carried out, the developed models are experimentally verified. This research, which is co–sponsored by ECSC and carried out at TNO Institute for Building Materials and Structures, comprises tests for studying the thermal behaviour and loading tests on complete flooring systems [8].
After verification of the model, practical design rules will be developed, for simple and rapid determination of the fire resistance. These rules will be proposed as revisions of the present European recommendations.
This paper deals with the numerical models as well as the experimental verification.

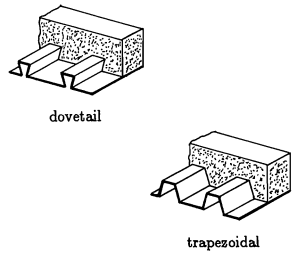

Fig.1 Composite steel/concrete slabs

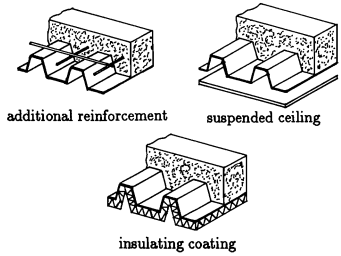

Fig.2 Fire–resistance measures

THERMAL ANALYSIS

A two–dimensional thermal model for the determination of temperature profiles in fire–exposed composite steel/concrete slabs has been developed. This model has been based on the finite difference method. It takes temperature–dependent material properties, evaporation of moisture, as well as arbitrary fire–exposure conditions into account.
For a detailed description of the thermal model, see references [5] and [6].

With regard to the thermal model a distinction is drawn between:
* the heat transfer from the fire to the slab (convection and radiation) and
* the heat transfer in the slab (conduction).

Heat transfer from the fire to the slab
The heat–transfer rate from the fire compartment to the slab is described in general formulas:

$$q = q_{con} + q_{rad} \quad (1)$$

$$q_{con} = \alpha_{con} A (T_{fire} - T_{sur}) \quad (2)$$

$$q_{rad} = \epsilon_{res} \sigma F A (T_{fire}^4 - T_{sur}^4) \quad (3)$$

with
q = total heat–transfer rate [W]
q_{con} = convective heat–transfer rate [W]
q_{rad} = radiative heat–transfer rate [W]
A = area [m²]
T_{fire} = air temperature in the fire compartment [K]
T_{sur} = surface temperature [K]
α_{con} = convective heat transfer coefficient [W/m²K]
ϵ_{res} = resulting emissivity [–]

σ = Stefan–Boltzmann coefficient
= $5.67 \cdot 10^{-8}$ W/m²K⁴
F = view factor [–]

α_{con} and ϵ_{res} are different for every fire compartment. These parameters should be experimentally determined. The view factor F indicates the influence of the position of the considered structural element in the fire compartment. For flat elements exposed to radiative heat transfer from all sides, the view factor equals 1 (e.g. the lower flange of the steel sheet). When the heat transfer is more or less obstructed, the view factor is less than 1 (e.g. the web and the upper flange of the steel sheet).

Heat transfer in the slab

The heat transfer and temperature throughout the whole structure are calculated for each time step. With regard to a rectangular discretisation with uniform dimensions, cf. Fig. 3, Fourier's differential equation, in finite difference notation yields:

$$\frac{\lambda_{i,j}[(T_{i+1,j} - T_{i,j}) - (T_{i,j} - T_{i-1,j})]}{\Delta x_i^2} + \frac{\lambda_{i,j}[(T_{i,j+1} - T_{i,j}) - (T_{i,j} - T_{i,j-1})]}{\Delta y_j^2} =$$

$$\rho_{i,j}\, c_{i,j}\, \Delta T_{i,j} / \Delta t \qquad (4)$$

with λ = conductivity [W/m·K]
ρ = specific mass [kg/m³]
c = specific heat [J/kg·K]
T = temperature [K]
Δx, Δy = dimensions of discretisation [m]
Δt = time step [s]
i, j = indices

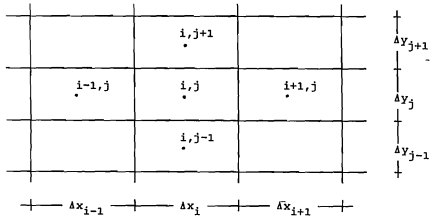

Fig.3 Rectangular discretisation with uniform dimensions

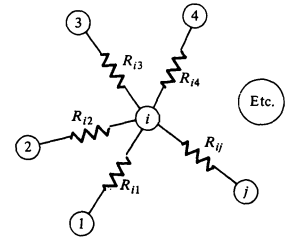

Fig.4 Heat capacities and resistances

In [5] the heat balance equations have been derived for other cases, such as nonrectangular discretisations. The heat transfer problem can be formulated by means of heat resistances and heat capacities, according to [9]. The capacities are concentrated in the nodes. The resistances are situated between the nodes, cf. Fig. 4.
The heat balance equations can be generally derived, as shown below.

$$q_i + \sum_j \frac{T_j^p - T_i^p}{R_{ij}} = C_i \frac{T_i^{p+1} - T_i^p}{\Delta t} \qquad (5)$$

with q_i = heat generation,c.q. dissipation in i (phase change) [W]
T^p_i = temperature of i after p time steps [K]
T^{p+1}_i = temperature of i after p+1 time steps [K]
T^p_j = temperature of adjacent element j after p time steps [K]
R_{ij} = heat resistance between i and j [K/W]
C_i = heat capacity of i [J/K]

Due to the rapid temperature rise in case of a fire, a rather short time step is necessary. Therefore an explicit solution method is appropriate for this kind of heat transfer problem. Formulating the heat transfer problem explicitly, the node temperatures at time p+1 can be directly derived from the temperatures at time p. Rewriting equation (5) leads to

$$T_i^{p+1} = T_i^p + \frac{\Delta t}{C_i}\left(q_i + \sum_j \frac{T_j^p - T_i^p}{R_{ij}} \right) \qquad (6)$$

To describe the thermal behaviour of a composite steel/concrete slab, the slab is discretised into rectangular, triangular and trapezoidal parts. The heat resistances between and capacities of these parts are determined and substituted in equation (6)

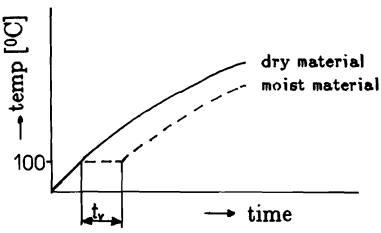

Fig. 5 Delay t_v in heating due to moisture

The heat transfer in the slab is influenced by the moisture content in the concrete. During heating a process of migration and evaporation of moisture takes place. For evaporation of the moisture present, a certain amount of energy is needed, thus retarding the heating process. This retardation of the heating is illustrated schematically in Fig. 5. In the model, it is assumed that the moisture evaporates as soon as a certain temperature is reached (e.g. 100°C). This assumption is normally appropriate in fire engineering calculations (e.g. [10]). The energy necessary for the evaporation, appears in equation (6) as q_i.

EXPERIMENTAL VERIFICATION THERMAL MODEL

In the scope of an international research program, co–sponsored by the European Coal and Steel Community (ECSC), the thermal model has been experimentally verified. Twelve test specimens of composite steel/concrete slabs have been tested with regard to the thermal behaviour during fire exposure. In each test specimen about 35 thermocouples have been situated in a number of cross–sections (lower flange, upper flange and intermediate sections). Different types of steel sheet have been considered, cf. Fig. 1. Further, the concrete depth has been varied. The thermal effect of the steel sheet has been studied in two specimens in which no steel sheet has been applied. To study the thermal behaviour separately, specimens with restricted length have been prepared. Six specimens were tested in one single test. The tests have been carried out at the Technical Centre for Fire Prevention of TNO Institute for Building Materials and Structures.
For a detailed description of the tests it is referred to [8], [11]. This section deals with the comparison of calculated and measured temperatures.

For two specimens with different types of steel sheet, the results are shown:
1 Super Holorib 51 with 70 mm concrete depth (dovetail type), cf. Fig. 7, and
2 Prins PSV 73 with 70 mm concrete depth (trapezoidal type), cf. Fig. 8.
The results are representative for all specimens tested.

In the calculations, the following parameters have been adopted:

1 Furnace temperatures
The heat transfer from the furnace to the slab is calculated on the basis of measured furnace temperatures (close to ISO–834 standard fire [1]).

2 Heat transfer parameters (convection and radiation)
With regard to the heat transfer from the furnace to the slab it is distinguished between convective and radiative heat transfer, with the following parameters:
- Convective heat transfer coefficient α_{con}
  - lower flange : 25 $W/m^2 \cdot K$
  - upper flange and web : 15 $W/m^2 \cdot K$
- Resulting emissivity ϵ_{res} of steel sheet
  With regard to radiative emissivity, a specific feature has to be highlighted. The sheet–steel surface consists of a thin galvanized layer which shows low emissivities for low temperatures. At temperatures of about 400–500°C, however, the zinc layer melts and the surface blackens. The emissivity increases in consequence of this phenomenon. Besides temperature, also temperature increase as function of time determines the speed of blackening. At high heating rates, the surface blackens at higher temperature.
  Considering these effects, the following resulting emissivities are chosen:
  - 0.1 for T<400°C
  - 0.4 for T>800°C
  - linear interpolation between 400 and 800°C
- View factor F
  - lower flange : 1
  - upper flange : 0.25 (Holorib), respectively 0.3 (Prins)
  - web : 0.4 (Holorib), respectively 0.6 (Prins)

3 Thermal material properties of concrete and steel

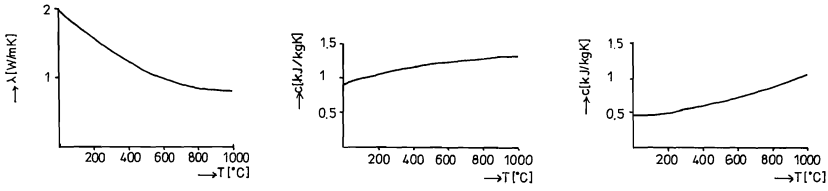

a) b) c)

Fig.6 Thermal properties of concrete and steel [12]:
a) conductivity λ_c of concrete
b) specific heat c_c of concrete
c) specific heat c_s of steel

Thermal material properties (conduction) of concrete and steel are adopted from [12], cf. Fig. 6:
* concrete
- $\rho_c = 2350$ kg/m³

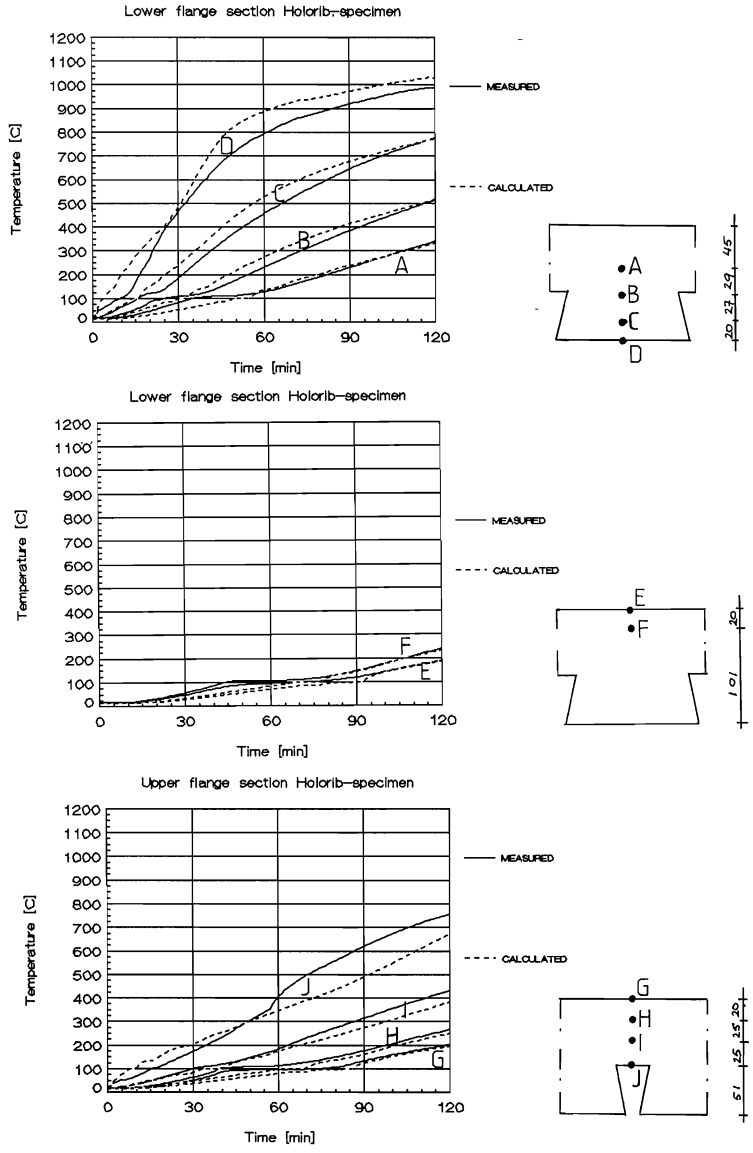

Fig. 7 Comparison of calculated and measured temperatures of Holorib specimen

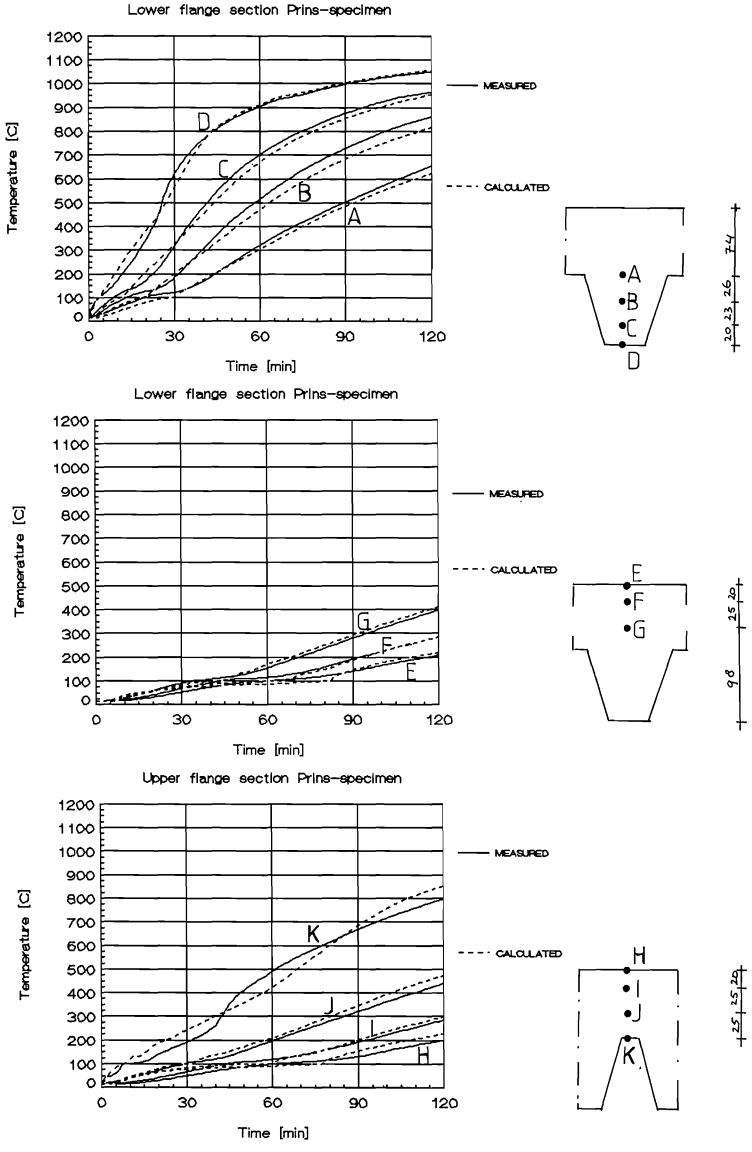

Fig. 8 Comparison of calculated and measured temperatures of Prins specimen

$$- \lambda_c = 2 - 0.24(\frac{T}{100}) + 0.012(\frac{T}{100})^2 \ \text{W/m·K} \quad (7)$$

$$- c_c = 900 + 80(\frac{T}{100}) - 4(\frac{T}{100})^2 \ \text{J/kg·K} \quad (8)$$

* steel

$$- \rho_s = 7800 \ \text{kg/m}^3$$

$$- c_s = 470 + 20(\frac{T}{100}) + 3.8(\frac{T}{100})^2 \ \text{J/kg·K} \quad (9)$$

4 Moisture content of concrete

The actual measured moisture contents have been applied in the calculations. These moisture contents vary between 2% (thin specimens) and 4% (thick specimens) by weight. For the specimens treated in this paper, the values were: 2.8% (Holorib), respectively 3.4% (Prins).

5 Heat transfer at nonexposed side

The following heat transfer parameters have been assumed:
- convective heat transfer coefficient α_{con}: 8 W/m²·K,
- view factor F: 1,
- resulting emissivity ϵ_{res} (concrete): 0.78.

The results are shown in Fig. 7 and 8. In view of the large uncertainties involved, especially the heat transfer phenomena during fire, the simulation result is quite good.

CROSS–SECTIONAL ANALYSIS

At room temperature, the cross–sectional behaviour of composite slabs is determined by the geometry and the mechanical properties of the components (profiled steel sheet, concrete and possibly reinforcement) and the method of construction (application of props). This behaviour is analysed on the basis of nonlinear elastic theory, assuming that plane sections remain plane after bending (Bernouilli) and a complete interaction between concrete and steel (no slip). The analysis yields an M–κ diagram, comprising both positive and negative bending as well as ascending and descending branches, cf. Fig. 9 (full line). The plastic moments M_p^- and M_p^+ as well as the flexural stiffnesses EI^- and EI^+ at room temperature (RT) have been indicated.

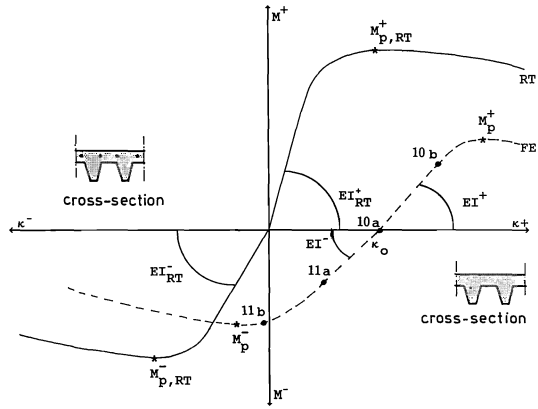

Fig. 9 The M–κ diagram for positive and negative bending. Comparison of room temperature (RT) and fire–exposure (FE) conditions

In comparison with room temperature, the cross–sectional behaviour of fire–exposed composite slabs changes due to the nonuniform temperature distribution in the cross–section. In each fibre of the cross–section, the temperature increase causes a thermal expansion and a decrease in strength and stiffness. In consequence of these changing material properties, thermal strains and stresses as well as a thermal curvature develop during fire exposure.

The nonuniform temperature distribution causes thermal strains that vary in two directions. For simplicity, only one dimension, the variation of strains with the height of the cross–section, is considered in this paragraph.

First, a nonloaded cross–section is considered (M=0). Owing to the nonuniform temperature distribution, a nonlinear (thermal) strain distribution would develop if all fibres could expand freely ($\epsilon_t = \alpha \cdot T$). However, according to Bernouilli's hypothesis, a linear strain distribution is assumed, partly restraining the thermal strains. This restraint causes thermal stresses, cf. the hatched area in Fig. 10.a. In the upper and lower parts of the cross–section compressive stresses occur, in the middle part tensile stresses. A thermal curvature κ_0 develops, for which the equilibrium conditions ($\Sigma H=0$ and $\Sigma M=0$) are fulfilled.

Second, a positive bending moment (M>0) is considered. The curvature κ increases beyond κ_0, cf. Fig. 10.b. The stress–related strains increase accordingly, compressive strains in the upper parts and tensile strains in the lower parts, cf. the hatched area in Fig. 10.b. The stress–related strains ϵ^σ are defined as the difference between the strains (according to the linear strain distribution) and the free thermal strains ($\alpha \cdot T$).

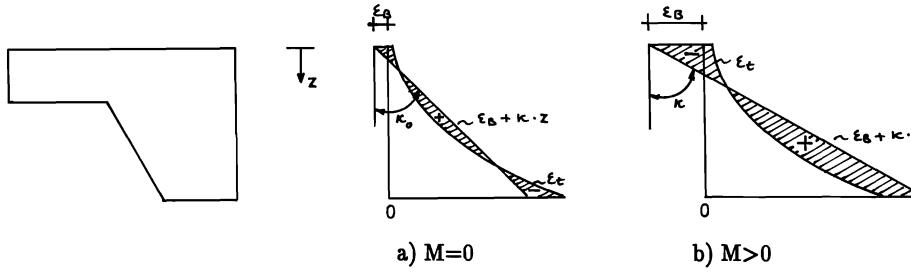

a) M=0 b) M>0

Fig.10 Strain distribution in cross–sections without load (a) and at positive bending (b)

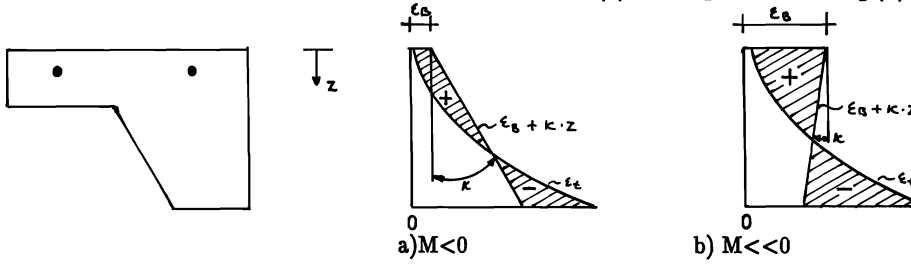

a)M<0 b) M<<0

Fig.11 Strain distribution in cross–sections at negative bending

Third, a negative bending moment ($M<0$) is considered. The curvature κ decreases below κ_0. First, between $\kappa=\kappa_0$ and $\kappa=0$, a negative bending moment corresponds to a positive curvature cf. Fig. 11.a. Then, below $\kappa=0$, a negative bending moment corresponds to a negative curvature cf. Fig. 4.b. The stress–related strains increase accordingly, compressive strains in the lower parts and tensile strains in the upper parts, cf. the hatched area in Fig. 11.

A characteristic M–κ diagram under fire–exposure is compared with that at room temperature, cf Fig. 9 (dotted line vs. full line). The points qualitatively described in Fig. 10 and 11 are indicated in Fig. 9. Plastic moments (M_p^- and M_p^+) and flexural stiffnesses (EI^- and EI^+) decrease as a function of fire–exposure time, while κ_0 increases.

STRUCTURAL ANALYSIS

On the basis of the M–κ diagrams, generated in the cross–sectional analysis, the structural behaviour is determined, yielding moment distributions and deflections as a function of time. Both statically determinate and statically indeterminate slabs can be analysed.

The determination of statically determinate slabs is fairly simple, as the moment distribution can be directly derived from the loading and the span. Therefore, the curvature distribution can be determined with the M–κ relations. From this, the deflections can be easily calculated.
In Fig. 12 the hypothetical case of linear elastic behaviour is presented. During fire exposure the stiffness EI decreases, causing larger deformations. Furthermore, deformations occur due to κ_0, that increases during fire exposure.
However, as the stiffness varies along the span, a nonlinear elastic model has to be applied.

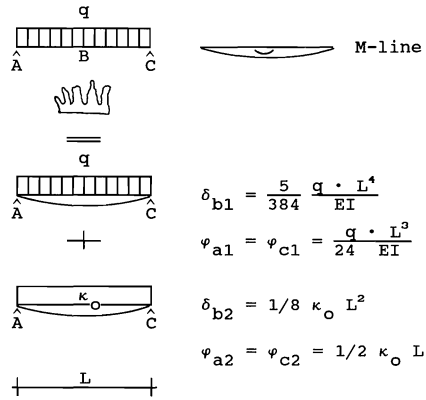

Fig.12 Simply supported slab (linear elastic behaviour)

Determination of the behaviour of statically indeterminate slabs is more complicated, because the moment distribution cannot be directly derived from the structural parameters (number and length of the spans, loading and supporting conditions). Moment distribution also depends on the stiffness distribution in the slab.
At room temperature a redistribution of moments takes place when the loading increases. For composite slabs, the nonlinear behaviour concentrates at the internal support sections. Accordingly, the stiffness of these sections decreases, yielding a relatively smaller contribution by the support moments to the load–bearing capacity , cf. Fig. 13. At a certain

load level, the negative plastic moment at the mid support is reached. Depending on the rotational capacity at this support, loading can be further increased, during which the moments at mid span may increase until the positive plastic moment is reached.

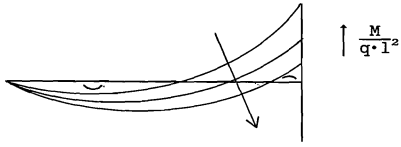

Fig.13 Redistribution of moments at room temperature

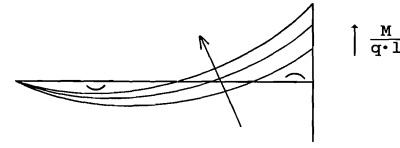

Fig.14 Redistribution of moments during fire exposure

During fire exposure, a redistribution of moments also takes place, although the load remains the same, cf. Fig. 14. Owing to the temperature increase, the flexural stiffnesses decrease and the thermal curvature κ_0 increases, cf. Fig. 9. Especially because of the latter effect, the support moment increases as a function of time, in contrast to the (relative) decrease during increased loading at room temperature, cf. Fig. 13 and 14.

In Fig. 15 the behaviour of a double–span continuous slab is schematically presented for the hypothetical case of linear elastic behaviour (constant stiffness of the whole slab). For reasons of symmetry, this static system can be substituted by a uniformly loaded simply supported slab with a support moment M_s acting at one support. A distinction is made between deformations due to the thermal curvature κ_0 , to the loading q and the support moment M_s. Compatibility requires the rotation at the mid support to be 0.
At an early stage of the fire, κ_0 has increased to such an extent that M_s reaches the negative plastic moment. Hence, analogously to room–temperature conditions, the rotational capacity of the support section is decisive for the load–bearing capacity. From negative bending tests at room temperature it is known that the rotational capacity can be primarily attributed to one (or two) major crack(s) appearing at the mid–support section [13]. The stated compatibility condition ($\Sigma\varphi_{support}=0$) does not hold any longer. Therefore the static system of Fig. 15 is no longer valid after major crack formation.
It has been shown that the rotational capacity of the mid–support section can, under circumstances, be satisfactorily predicted assuming a constant moment area of approximately 100 mm at the mid support [13].
Under fire conditions, the rotational capacity is also simulated by choosing an appropriate length of the constant moment area.
The rotational capacity problem of a double–span continuous slab has thus been schematized as a triple–span continuous slab of which the (small) fictitious span represents the mid–support section of the actual slab, providing the rotational capacity, cf. Fig. 16. For symmetry reasons this static system can be substituted by a simply supported slab AB with a cantilever BC and a moment M_s at the end of the cantilever C. M_s is the constant moment acting at the mid–support section BD of the triple–span slab. Actual values of the length of the constant moment area are to be derived from calculations with a discrete crack model [14] and from experiments.

The hypothetical case of constant stiffnesses for each span does not occur. The stiffness varies along the span, which is the reason why a nonlinear elastic model has to be applied. Furthermore, an iteration process is necessary, in which the support moment and the stiffness distribution are determined in such a way that the compatibility condition is fulfilled.

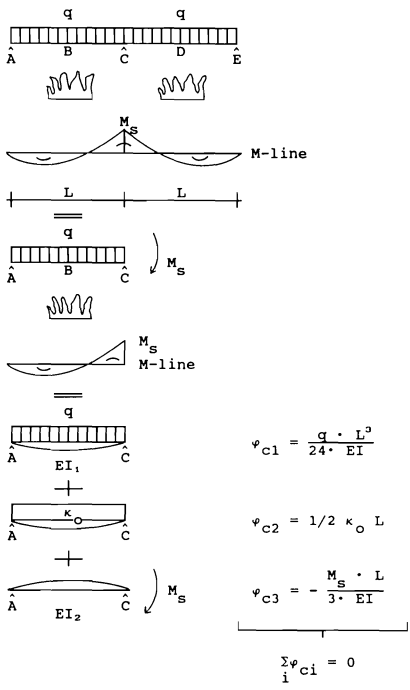

Fig.15 Continuous slab (constant stiffness of the whole slab)

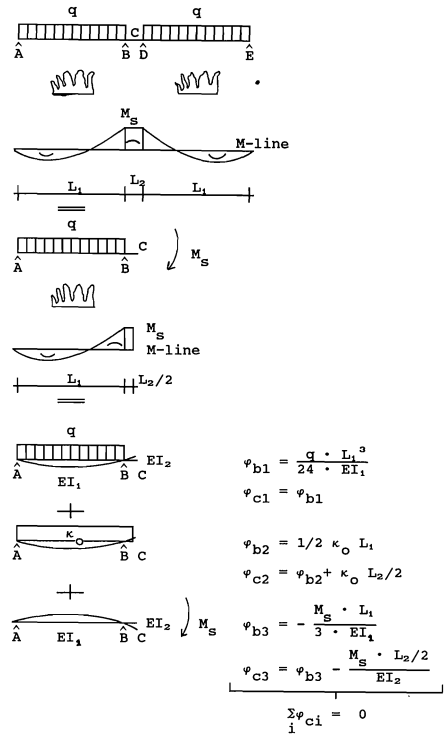

Fig.16 Continuous slab with a constant moment area (constant stiffnesses of each span)

EXPERIMENTAL VERIFICATION MECHANICAL MODEL

The mechanical model is being experimentally verified by means of fire tests on complete (loaded) systems. Three kinds of tests are carried out:

1 Simply supported slabs
Two tests on simply supported slabs are carried out to study the behaviour under positive bending.

2 Cantilever slabs
Three tests on cantilever slabs are carried out to study the behaviour under negative bending. The tests have been designed to study the behaviour of a mid–support section of a continuous slab. To consider redistribution of moments, the deformation of the cantilever is controlled. This is done on the basis of calculations with the model on continuous slabs. With the tests, also information is obtained with regard to the rotational capacity.

3 Continuous slabs
Six tests on (double–span) continuous slabs are carried out. With the tests on simply supported and cantilever slabs, parts of a continuous slab can be separately studied. With the tests on continuous slabs the global behaviour is analysed.

Besides the static system, the application of additional reinforcement (positive as well as negative) is varied in the tests.

This paper deals with the experimental verification of the positive bending behaviour on the basis of tests on simply supported slabs (cf. 1). Tests on cantilever and continuous slabs (cf. 2 and 3), are currently being performed and will be reported in the near future.
The results of one of the tests are given and compared with calculation results. Information with respect to this test:

- Prins PSV 73 profiled steel sheet,
- 70 mm concrete depth (total depth 143 mm),
- shrinkage mesh (ϕ6–150) at 20 mm distance from top of slab,
- additional positive reinforcement: 1ϕ10 bar in every 2 troughs (0.32% reinforcement ratio), positioned in the centre of the trough at the height of the upper flange of the steel sheet, cf. Fig. 17,
- standard fire conditions [1],
- axial restraint at the supports has been excluded, by suspending the slab at one of the supports,
- span L=3200 mm,
- loading q=5.8 KN/m^2, consisting of 2.8 KN/m^2 dead weight and 3 KN/m^2 imposed loading.

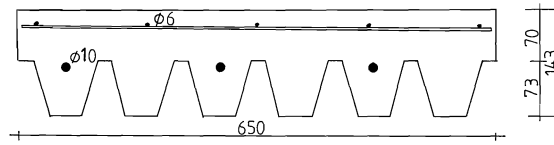

Fig.17 Cross–section of tested Prins specimen

In the calculation, the following parameters have been adopted:

1 Temperatures
Temperatures calculated with the thermal model, that show good agreement with measured temperatures, cf. Fig. 8, are applied. Generally, a good description of the temperature development is important with regard to thermal curvature, which has a large influence on the total deformation behaviour. More specifically, a good description of the temperature of the positive reinforcement (cf. A in Fig. 8) is important with regard to failure and the deformation behaviour near failure.

2 Thermal expansion
Thermal expansion of concrete and steel have been adopted from [12], cf. Fig. 18.

3 Mechanical properties at room temperature
– concrete: compressive strength: 25 N/mm^2,
– steel sheet: yield stress 280 N/mm^2,
– reinforcement: actual measured values :

	positive	negative
yield stress R_e	587 N/mm^2	552 N/mm^2
ultimate stress R_m	677 N/mm^2	598 N/mm^2
strain at R_m	12.5%	5.0%

4 Mechanical properties at elevated temperatures
Mechanical properties of concrete and steel at elevated temperatures have been adopted from [12], cf. Fig. 19 to 21. For steel material laws for structural steel have been taken. For the reinforcing steel, the decrease of the ultimate stress R_m at

elevated temperatures has been differently adopted: conform values, obtained from tests on Tempcore reinforcement [15]. This decrease appeared to be higher for temperatures beyond 400°C.

In Fig. 22 calculated and measured deflections at mid span are compared to each other. The agreement is satisfactory.

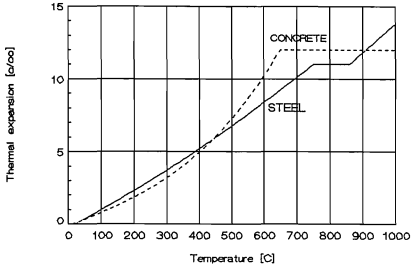

Fig.18 Thermal strain of steel and concrete [12]

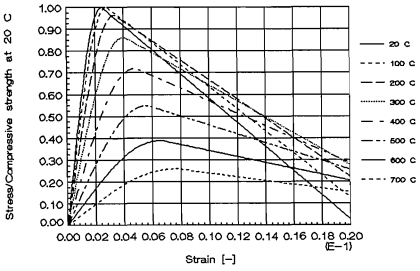

Fig.19 σ–ϵ (T) diagram of concrete [12]

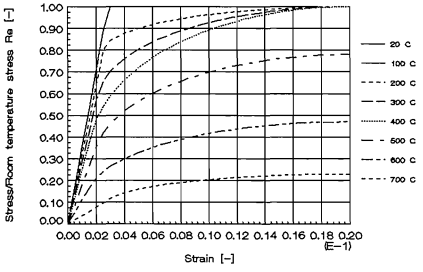

Fig.20 σ–ϵ (T) diagram of steel sheet [12]

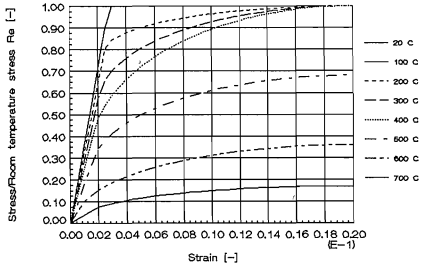

Fig.21 σ–ϵ (T) diagram of reinforcement [12]

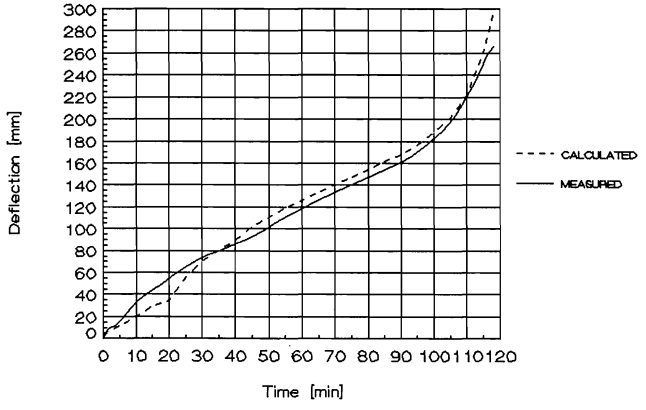

Fig. 22 Comparison of measured and calculated mid–span deflections

CONCLUSIONS

On the basis of the comparisons of calculated and measured temperatures, it can be concluded that the thermal model gives a satisfactory prediction of the heating behaviour of fire–exposed composite steel/concrete slabs.
On the basis of the comparisons of calculated and measured deflections of simply supported slabs, it can be concluded that the positive bending behaviour is satisfactorily predicted by the mechanical model.
In the near future, the negative bending behaviour will be studied on the basis of tests on cantilever slabs, the global behaviour on the basis of tests on continuous slabs.

ACKNOWLEDGEMENT

This paper was co–sponsored by the Netherlands Organization for Scientific Research (NWO).

APPENDIX 1: REFERENCES

1. International Standard ISO 834, Fire resistance test–elements of buildings construction, 1975.
2. CEB, Model code for fire design of concrete structures. Bulletin d'Information CEB no.174, 1987.
3. ECCS, Committee T3–Fire safety of steel structures, European recommendations of the fire safety of steel structures, Elsevier, 1983.
4. ECCS, Committee T3–Fire safety of steel structures, Calculation of the fire resistance of composite concrete slabs with profiled steel sheet exposed to the standard fire, technical note, 1983.
5. Hamerlinck, A.F., A thermal model for the calculation of fire–exposed composite steel/concrete slabs (in Dutch). Eindhoven University of Technology, Faculty of Architecture, Building and Planning, Bouwstenen 13, 1988.
6. Hamerlinck, A.F., A thermal model for fire–exposed composite steel/concrete slabs. Numerical Methods in Thermal Problems, volume VI, pp. 1401–1411, 1989.
7. Hamerlinck, A.F., A mechanical model for the calculation of fire–exposed composite steel/concrete slabs. Eindhoven University of Technology, Faculty of Architecture, Building and Planning, report TUE–BKO–KO–90.01, 1990.
8. Hamerlinck, A.F., Twilt, L., ECSC sponsored research on the behaviour of fire exposed composite steel/concrete slabs. TU Eindhoven/TNO Delft, report BI 89–016, 1989.
9. Holman, J.P., Heat transfer, McGraw–Hill Book Company, 1986.
10. Franssen, J.–M., Etude du comportement au feu des structures mixtes acier–béton, Université de Liège, Faculté des sciences appliquée, 1986.
11. Hamerlinck, A.F., Twilt, L., The thermal behaviour of fire–exposed composite steel/concrete slabs, test report, draft. Eindhoven University of Technology/TNO Delft, 1990.
12. Eurocode 5: Composite structures, Part 10: Structural fire design, 5th draft, 1989.
13. Vliegen, J.P.F.M., The behaviour of statically indeterminate composite steel/concrete slabs (in Dutch). Eindhoven University of Technology, report TUE–BKO–88.12, 1988.
14. Hamerlinck, A.F., The rotational capacity of statically indeterminate composite steel/concrete slabs. Eindhoven University of Technology, Faculty of Architecture, Building and Planning, report TUE–BKO–KO–90.02, 1990.
15. Ruge, J., Winkelmann, O., Linnemann, R., Verformungsverhalten von Bau–, Beton– und Spannstählen bei hohen Temperaturen, TU Braunschweig, SFB 148 "Brandverhalten von Bauteilen", Arbeitsberichte 1978–1986.

APPENDIX 2: NOTATION

Thermal analysis:

α_{con} = convective heat transfer coefficient [W/m^2K]
$\Delta x, \Delta y$ = dimensions of discretisation [m]
Δt = time step [s]
ϵ_{res} = resulting emissivity [–]
λ = conductivity [$W/m \cdot K$]
ρ = specific mass [kg/m^3]
σ = Stefan–Boltzmann coefficient
= $5.67 \cdot 10^{-8}$ W/m^2K^4

A = area [m^2]
C_i = heat capacity of part i [J/K]
c = specific heat [$J/kg \cdot K$]
F = view factor [–]
i, j = indices with regard to space discretisation
p = index with regard to time discretisation
q = total heat–transfer rate [W]
q_{con} = convective heat–transfer rate [W]
q_{rad} = radiative heat–transfer rate [W]
q_i = heat generation,c.q. dissipation in part i (phase change) [W]
R_{ij} = heat resistance between parts i and j [K/W]
T = temperature [K]
T_{fire} = air temperature in the fire compartment [K]
T_{sur} = surface temperature [K]
T_i^p = temperature of part i after p time steps [K]
T_i^{p+1} = temperature of part i after p+1 time steps [K]
T_j^p = temperature of adjacent element j after p time steps [K]

Mechanical analysis:

α = coefficient of thermal expansion [K^{-1}]
ϵ_t = thermal strain (free expansion) = $\alpha \cdot T$ [–]
ϵ^σ = stress–related strain [–]
κ = curvature [m^{-1}]
κ_0 = thermal curvature (for M=0) [m^{-1}]
φ = rotation [rad]

EI^+ = flexural stiffness under positive bending [$N \cdot m^2$]
EI^- = flexural stiffness under negative bending [$N \cdot m^2$]
L = span [m]
M = moment [$N \cdot m$]
M_p^+ = positive plastic moment [$N \cdot m$]
M_p^- = negative plastic moment [$N \cdot m$]
M_s = support moment [$N \cdot m$]
q = loading [N/m^2]
R_e = yield stress [N/mm^2]
R_m = ultimate stress [N/mm^2]
T = temperature [K]